Wind and Structures, *Vol. 27, No. 4 (2018) 213-221*
DOI: https://doi.org/10.12989/was.2018.27.4.213

The motion rule of sand particles under control of the sand transportation engineering

Lin-gui Xin, Jian-jun Cheng*, Bo-yu Chen and Rui Wang

College of Water Resources and Architectural Engineering, Shihezi University, Shihezi Xinjiang 832003, China

(Received December 6, 2017, Revised July 5, 2018, Accepted July 10, 2018)

Abstract. In the desert and Gobi regions with strong wind and large sediment discharge, sand transporting engineering is more effective than sand blocking and sand fixing measures in sand prevention. This study uses the discrete phase model of 3D numerical simulation to study the motion trail, motion state and distribution rule of sand particles with different grain diameters when the included angle between the main shaft of the feather-row lateral transportation sand barrier and the wind direction changes, and conducts a comparison in combination with the wind tunnel test and the flow field rule of common sand barrier. According to the comparison, when wind-sand incoming flow passes through a feather-row sand barrier, sand particles slow down and deposit within the deceleration area under the resistance of the feather-row sand barrier, move along the transportation area formed by the transportation force, and accumulate as a ridge at the tail of the engineering. With increasing wind speed, the eolian erosion of the sand particles to the ground and the feather-row sand barrier is enhanced, and the sand transporting quantity and throw-over quantity of the feather-row sand barrier are both increased. When sand particles with different grain diameters bypass the feather-row sand barrier, the particle size of the infiltrating sands will increase with the included angle between the main shaft of the feather-row sand barrier and the wind direction. The obtained result demonstrates that, at a constant wind speed, the flow field formed is most suitable for the lateral transportation of the wind-drift flow when the included angle between the main shaft of the feather-row sand barrier lateral transportation engineering and the wind speed is less than or equal to 30°.

Keywords: 3D numerical simulation; discrete phase model; wind-sand two-phase flow; lateral transportation; rule of motion

1. Introduction

China is among the countries with the largest desert area in the world. China's deserts are mainly distributed in the northwest, the north of North China, and the west of the Northeast (above 35th parallel north). Here, major deserts include the Taklimakan Desert, the Gurbantunggut Desert, and the Tengger Desert, covering an area of more than 100 km2. Desertification is a severe environmental issue current threatening ecosystems around the world. It severely affects the survival of humans and the sustainable development of the society. Desertification not only threatens the entire living environment of all humans, but also restricts global economic development and social stability. Furthermore, with increased desertification, sand disasters including wind-drift sand movement and sand dune migration are increasingly hazardous to railways and roads. Various wind and sand prevention measures must be taken so that the resulting sand damage can be effectively relieved (Li and Lei 2003, Huang *et al*. 2013, Tian *et al*. 2015, Rezaie 2009, Murai *et al*. 1990, Gumaa *et al*. 1998, Li and Sherman 2015, Cheng *et al*. 2016a, Cheng *et al*. 2016b, Lima *et al*. 2017, Mcclure *et al*. 2017). In response to unidirectional wind, when the wind power is strong and the sand source is rich, the adoption of simple sand blocking and sand fixing measures can only control the sand damage for a short period. However, when the sand particles in front of the sand barrier sharply increase with time, the sand blocking function of the sand barrier declines and will even increase the resulting sand damage. Therefore, taking advantage of both vantage ground and wind power to use transportation measures will be more effective than such sand blocking and sand fixing measures. A feather-row lateral transportation barrier is mainly applied to sections with abundant sand resources. Furthermore, it is allied where the transport line is parallel to or has a small skew angle with the prevailing wind direction. Here, it is advisable to change the airflow direction to transport the wind-drift sand to both sides instead of the transport line itself (Fig. 1).

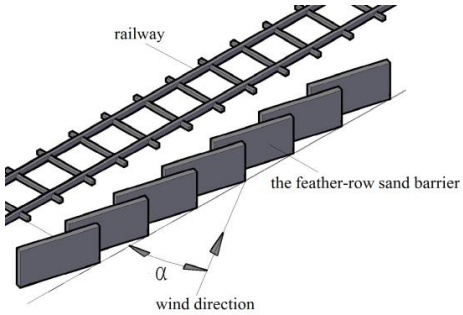

Fig. 1 Schematic diagram of the feather-row sand barrier

*Corresponding author, Professor
E-mail: chengdesign@126.com

Copyright © 2018 Techno-Press, Ltd.

ISSN: 1226-6116 (Print), 1598-6225 (Online)

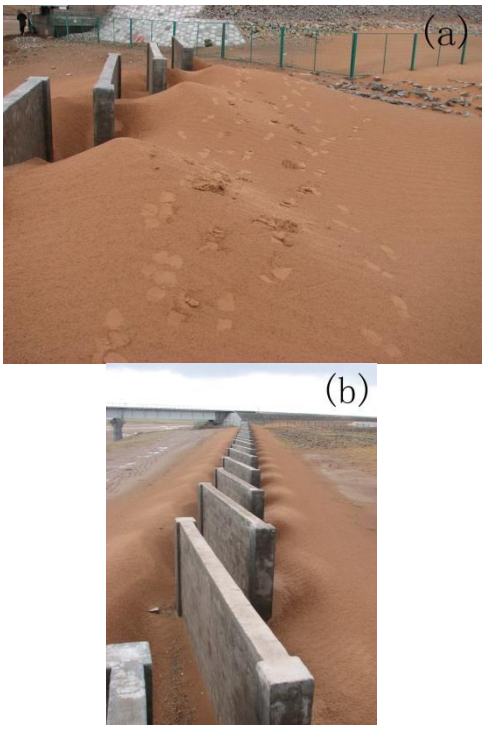

Fig. 2 Practical application of the feather-row transportation engineering

Eolian sand movement is a complex gas-solid two-phase flow motion. The simulation model that has been dedicated to the research of eolian sand movement has been constantly improved. Currently, the model with the closest simulated result to the actual situation of eolian sand movement is the discrete phase model (DPM) (Chen *et al.* 2014, Li *et al*. 2014a, Li *et al.* 2014b, Sun *et al*. 2001, Paz *et al.* 2015.). Significant scientific studies have investigated the motion trail and the way of sand particles. For example, Kang *et al*. (2011) studied the motion trail of sand particles. Mcewan *et al*. (2010) studied the collision of sand particles. Sterk *et al*. (1998) studied the sand transport rate during saltation. Based on existing research theories and the results of numerical models, this study used the discrete phase model to investigate the motion rule of wind-drift sand in the feather-row lateral transportation sand barrier. The aim was to provide a theoretical basis for the application of the feather-row lateral transportation engineering, while avoiding abnormal sand deposit status shown in Fig. 2 in actual engineerings.

2. Numerical simulation method

2.1 Modeling

A 3D model of the feather-row engineering was established in the ANSYS Design Moder as shown in Fig. 3. The size of the computational domain was 150 m × 30 m × 20 m. The distance between the feather-row engineering and the inlet was 75 m. According to the structural features of the wind-drift sand, the layer was at a height of 2 m at the inlet. The medium of the upper inlet was air while the media of the lower inlet were air and sand. The size of a single feather-row is 4 m × 2 m × 0.2 m. Both their overlapping length and the gap between adjacent feather-row are 0.5 m and the included angles (α) between the main shaft of the feather-row engineering and the wind direction were 30°, 45°, and 60°, respectively.

2.2 Mesh partition

Since the fluid computational domain model of the feather-row engineering is asymmetrical and relatively complicated, Tetrahedrons mesh partition was adopted in the grid partition. Patch Independent was chosen as algorithm, as it favors the smoothing, node combination, and edge exchange of the volume mesh and the table mesh, the coarsening of separate areas, as well as local refining and coarsening to the computational domain. To control the computational accuracy, mesh refinement was conducted to the ground area and inflation refinement was adopted for the feather-row engineering. The smoothing transformation method was used and the refined mesh has five layers and an increase rate of 1.2. The result of the obtained grid partition is shown in Fig. 4.

2.3 Boundary conditions and parameter setting

The simulated condition used for this study was that wind blows the sand. In accordance with the principle of aerodynamics, this indicates incompressible flow with a mach number below 0.3.

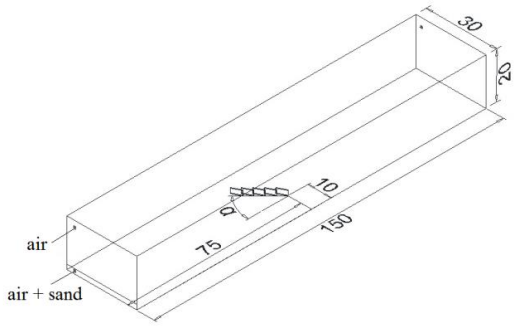

Fig. 3 Schematic diagram of the computational domain

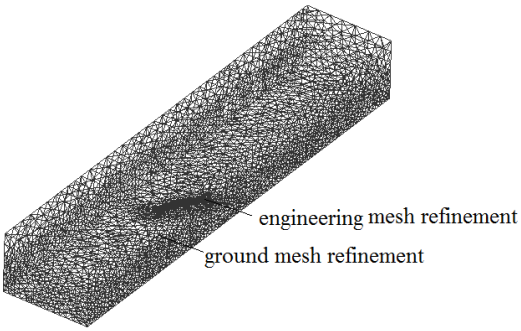

Fig. 4 Schematic diagram of mesh partition of the computational domain

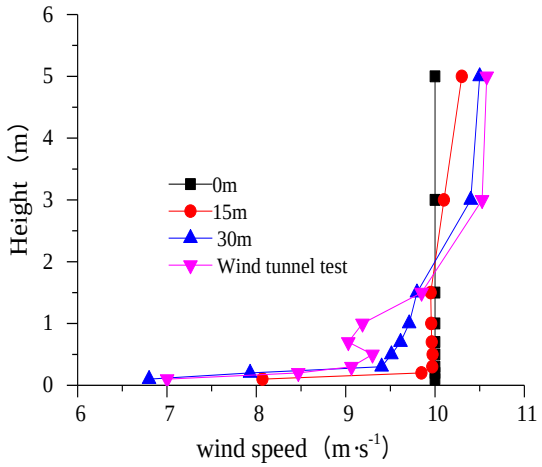

Fig. 5 Variation rule of wind velocity profile in numerical model

This mach number indicates that the inlet condition of the model is a velocity-inlet. Because free effluent is only adopted when the flow state develops fully and the model inlet cannot guarantee free effluent, the inlet condition of the model is that of a pressure-outlet, and the differential pressure is 0 (Patankar and Joseph 2001).

Based on actual working conditions, the actual situation of the upper boundary follows a borderless atmospheric surface; therefore, the boundary condition is that of a pressure-outlet with a differential pressure of 0. The roughness of the other boundary conditions is that of a wall and the lower boundary and the feather-row is the default condition. The roughness of both the right and left boundaries is 0. Because the sand phase is defined as a discrete phase, for particle flow, the boundary condition of the lower boundary and the feather-row is reflect and other boundary condition is escape. Wind-drift sand is represented by the motion of dense sand particles under the effect of the wind field, which is a typical two-phase flow. The discrete phase model uses a continuous phase air and the sand particles are inert jet particles. The jet plane is the velocity inlet below and the coupling between particles and the continuous phase can describe the motion trail of the sand particles well. A standard k-ε turbulence model is attached according to Rocha *et al.* (2014). The turbulence intensity I is 0.05, the turbulence radius R is 1 m, and the Syamlal-O'Brien drag force model was chosen. The utilized equation set solving algorithm is the SIMPLEC algorithm. The simulated wind velocity is 8 $m \cdot s^{-1}$, 10 $m \cdot s^{-1}$, and 12 $m \cdot s^{-1}$, respectively.

2.4 Numerical model method and verification

The simulation of the wind sand two phase flow in the CFD software mainly adopts its own discrete phase model (DPM), which is based on the Euler-Lagrange method. It models the fluid as a continuous medium, which is described in the Eulerian coordinate system. Consequently, it solves the transport equation in a continuous phase and uses the sand particle group as a discrete system. Therefore, we can get the orbit of the particles and calculate the energy transfer caused by particles through the differential equation of the particle force in the integral Lagrange coordinate system. Furthermore, in the calculation, the influence of interphase coupling and coupling results on the discrete phase orbit and the continuous phase flow can be integrated. When calculating the orbit of particles, CFD tracking calculates the gain and loss of particles mass and momentum along the track. These physical quantities can act on the calculation of the subsequent continuous phase. As a result, the effect of the discrete relative continuous phase can be considered, while the continuous phase affects the discrete phase. Alternatively, the governing equations of the dispersed phase and the continuous phase are solved alternately until both are all convergent (i.e., the two calculation solutions no longer change).

Based on the selection of the computing domain, the division of meshes, and the setting of parameters, the inlet wind speed was set to uniform flow speeds of 8 $m \cdot s^{-1}$, 10 $m \cdot s^{-1}$, and 12 $m \cdot s^{-1}$, respectively. For a wind speed of 10 $m \cdot s^{-1}$, the wind speed profile at a distance to the inlet of 0 m, 15 m, and 30 m is shown in Fig. 5. To verify the accuracy of the numerical model, the profile wind speed was measured in a wind tunnel test. Because the uniform flow at the entrance is affected by conditions such as surface roughness and boundary layer, it will gradually develop into profile flow and basically coincide with the measured profile wind speed in the wind tunnel test. Therefore, the numerical model can be used to study the motion rule of sand particles under the control of feather-row engineering.

3. Result and analysis

3.1 Features of the flow field around the feather-row engineering

By numerical simulation, both the common sand barrier and the feather-row engineering were chosen (the included angle between the main shaft and the wind direction is 30°), these are highly identical examples. For a wind velocity of 10 $m \cdot s^{-1}$, the cross section in the middle of the computational domain was chosen (x = 15 m) and the cross section at 0.5 m above the ground (z = 0.5 m) along the vertical and horizontal directions. A flow field comparison between the common sand barrier and the feather-row engineering is shown in Fig. 6. Due to the velocity change in the flow field, in the vertical direction, the flow field in front of common sand barrier can be divided into a backflow area and a deceleration area, while the feather-row engineering mainly has a deceleration area only. In the horizontal direction, the flow field in front of the common sand barrier can be divided into a deceleration area and a backflow area, while the feather-row engineering can be divided into a transportation area and a deceleration area.

The wind tunnel experiment for the common sand barrier was conducted at the Wind Tunnel Laboratory of the Cold and Arid Regions Environmental and Engineering

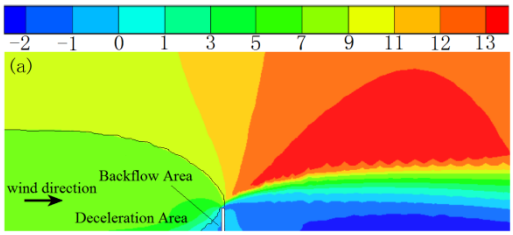

(a) Vertical flow field of common sand barrier

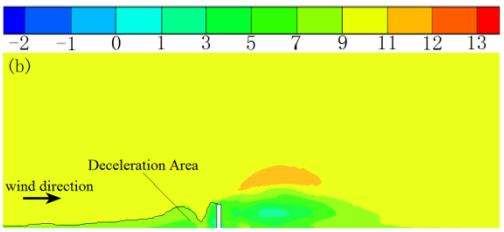

(b) Vertical flow field of the feather-row engineering

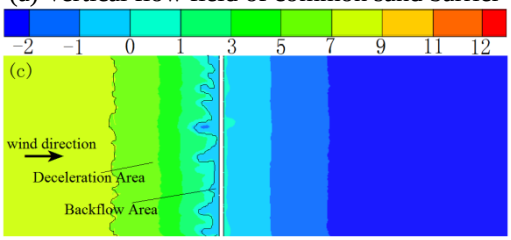

(c) Horizontal flow field of common sand barrier

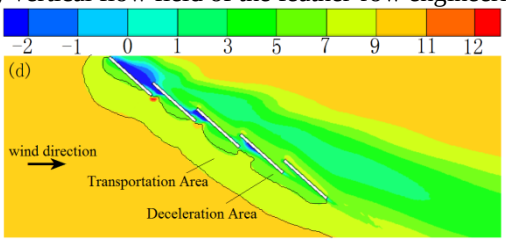

(d) Horizontal flow field of the feather-row engineering

Fig. 6 Flow field velocity distributions of common sand barrier and the feather-row engineering when the wind velocity is 10 m·s^{-1}

(a) The wind velocity is 8 m·s^{-1}

(b) The wind velocity is 10 m·s^{-1}

(c) The wind velocity is 12 m·s^{-1}

Fig. 7 Sand accumulation forms of common sand barrier at different wind velocity

Research Institute of the Chinese Academy of Sciences. The length of the wind tunnel is 38 m and the length of the experimental section is 21 m and the cross section of the wind tunnel is 1.2×1.2 m. The wind tunnel is composed of five parts: a power section, a rectifying section, a sand supplying device, an experimental section, and a diffusion section. To ensure sufficient strength and stiffness, the real sand barrier model was made of PVC materials. The height H of the model is 20 cm and the length L is 110 cm. During the wind tunnel experiment, the sand accumulation tests of the common sand barrier at wind velocities of 8 m·s^{-1}, 10 m·s^{-1}, and 12 m·s^{-1} are shown in Fig. 7. When the sand resource was abundant, the accumulated sand quantity in front of the common sand barrier increased with increasing wind velocity. For a wind velocity of 12 m·s^{-1}, several sand piles accumulated at the back of common sand barrier. The sand accumulation rule of the common sand barrier conforms to the flow field features of the numerical simulation. A comparison between the flow field distribution and the wind tunnel experiment of the common sand barrier showed that when sand particles move into the effective range of the common sand barrier, they will slow down in the deceleration area and deposit in the backflow area. Because of the existence of the transportation area in the feather-row engineering, the sand particles will change direction in the transportation area and continue to move. Therefore, the main function of the common sand barrier is to block and fix the sand while the function of the feather-row engineering is to transport the wind-drift sand.

3.2 Motion rule of sand particles

The change of the included angle between the main shaft of the feather-row engineering and the wind direction will sharply change the features of the flow field and sand accumulation around the feather-row, further influencing the width and length of its protection area. Therefore, the study of the change of the included angle between the main shaft of the feather-row and the wind direction is of vital significance to guide the formation mechanism of its surrounding flow field speed. Based on the DPM model, the saltation movement of the wind-drift sand was studied and the size of the sand particle was defined as 0.2 mm. For a wind velocity of 10 m·s^{-1}, the included angles between the main shaft of the feather-row engineering and the wind direction are 30°, 45°, and 60°. The motion trail of the sand particles in the flow field is shown in Fig. 8.

After saltation movement, the sand particles reach the deceleration area in front of the feather-row engineering, where they gradually slow down. Here, they are divided

into three parts: The first part that deposits around the feather-row as a result of the influence of the backflow area and the wall effect of the feather-row. The second part is affected by the airflow when passing the blocking wall and moves over the feather-row toward the protection area. The third part passes the feather-row and continues to move toward the next feather-row along the transportation direction in front of the feather-row, finally accumulating in the shape of a ridge at the tail of the engineering.

However, with increasing included angle between the main shaft of the feather-row engineering and the wind direction, the quantity of the sand particle accumulating at the feather-row also increases. For example, Fig. 8 shows that for an included angle of 30°, the accumulating quantity is small (almost 0). When the included angle is 45°, the accumulating quantity increases gradually and a small part of the sand particles accumulates at the feather-row engineering. For an included angle of 60°, a large quantity of sand particles accumulates at the feather-row engineering and moves toward the protection area. The reason why the accumulating quantity increases is that the real sand barrier is a bluff body with sharp edges and when passing through the sand barrier, the airflow is squeezed at the top and thus separates, forming a strong shear layer (Andrew and Gary 1996). The pressure difference between both sides of the shear layer is deflected at the flow line and returns to the separation area when the airflow is close to the ground, thus compensating the part of airflow removed via air engulfment (Lee *et al.* 2002, Jackson *et al.* 2013). A bigger included angle between the main shaft of the feather-row and the wind speed strengthens the shear layer it forms. Furthermore, the quantity of the sand particles accumulating at the feather-row engineering also continues to increase. Therefore, a smaller included angle between the main shaft of the feather-row and the wind direction improves the transportation of the wind-drift sand.

The major factor influencing the motion trail of sand is the change of the resistance caused by the change of the included angle between the main shaft of the feather-row and the wind direction. The resistance on the side of the feather-row facing the wind is Nx and the transportation force perpendicular to Nx is Ny. The numerical value of the resistance Nx and the transportation force Ny change with the wind velocity and the resulting angles are shown in Table 1.

Table 1 Acting force change table of the feather-row when the included angle changes

Included Angl	Acting Force (N)					
	Nx			Ny		
	Wind Velocity (m·s^{-1})					
(°)	8	10	12	8	10	12
30	914	1,427	2,046	979	1,522	2,181
45	1,250	1,980	2879	837	1,330	1,930
60	1,446	2,284	3,321	477	753	1,091

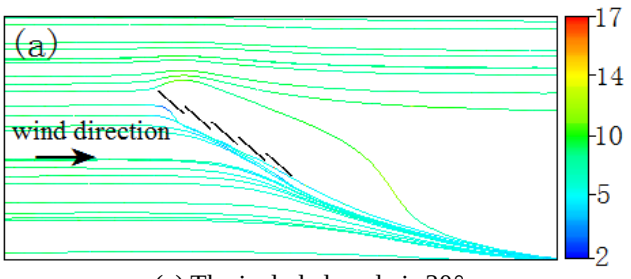

(a) The included angle is 30°

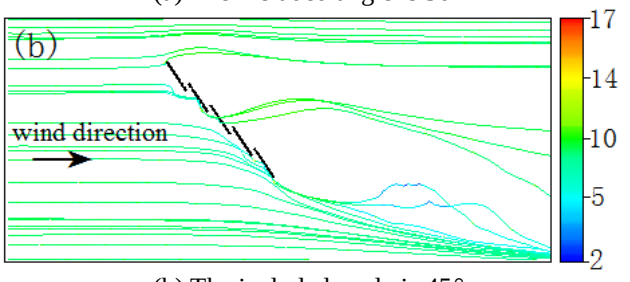

(b) The included angle is 45°

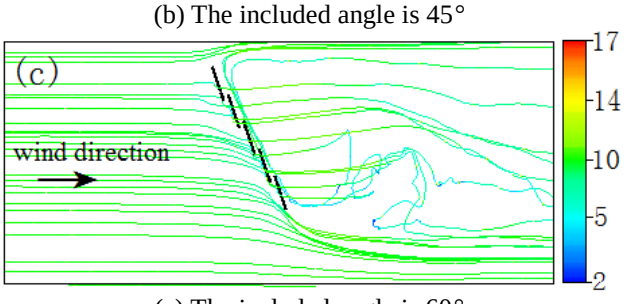

(c) The included angle is 60°

Fig. 8 Velocity contour of sand particles passing through the feather-row engineering when the wind velocity is 10 m·s^{-1}

The above-mentioned flow field analysis indicates that the change of the included angle between the main shaft of the feather-row engineering and the wind direction will change the engineeringed area of the feather-row engineering on the surface facing the wind.

Therefore, the engineeringed area of the feather-row engineering on the surface facing the wind also increases with increase included angle. The resistance Nx continued to increase, while the transportation force Ny decreased. As a result, the accumulating quantity of the sand particles when passing through the feather-row engineering increased. A comparison of the data showed that for an included angle between the main shaft of the feather-row engineering and the wind direction of 60°, the resistance Nx far exceeds the transportation force Ny. For an included angle of 45°, the distance between them is shortened; however, the resistance Nx is still exceeds the transportation force Ny. For an included angle of 30°, the transportation force Ny exceeds the resistance Nx, which means that the included angle between the main shaft of the feather-row engineering and the wind direction of 30° is best for the transportation of the sand. Analyzing of the increasing trend of the resistance Nx and the decreasing trend of the transportation force Ny suggested that with the increase of the included angle, the data difference from 30° to 45° is less than that form 45° to 60°. This demonstrates that with the decrease of the included angle between the

main shaft of the feather-row engineering and the wind direction, the influence of the feather-row engineering on the resistance Nx and the transportation force Ny continually decreases. Because of this and considering the engineering budget, the included angle between the main shaft of the feather-row engineering and the wind direction can be increased accordingly. In combination with practical engineering needs, the width of the protection area can be enlarged and the cost performance of the engineering can be enhanced.

Saltation movement is the major form of motion for sand particles in wind-sand two-phase flow. The sand particles in saltation movement are affected by the uplifting force of the wind and accelerate after having obtained their kinetic energy from the airflow. With increasing wind velocity, the numerical value of the wind velocity of the flow field around the feather-row engineering changes accordingly, influencing the form and direction of motion of sand particles (Tanière *et al*. 1997). Based on the DPM washout model, the included angle between the main shaft of the feather-row engineering and the wind direction was set to 30°. For wind velocities of 8 $m \cdot s^{-1}$, 10 $m \cdot s^{-1}$, and 12 $m \cdot s^{-1}$, the eolian situation of the saltation movements are shown in Fig. 9.

As shown in Fig. 9, for a wind velocity of 8 $m \cdot s^{-1}$, sand particles that fall onto the ground continue to move due to the effect of bounce.

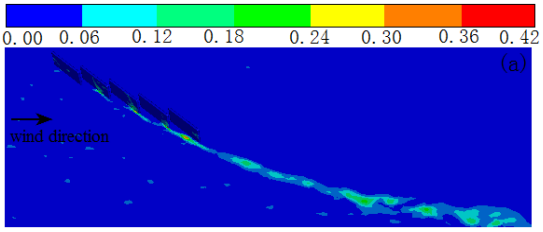

(a) The wind velocity is 8 $m \cdot s^{-1}$

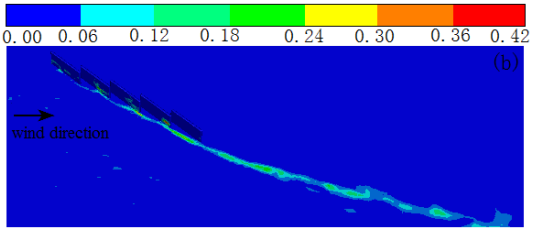

(b) The wind velocity is 10 $m \cdot s^{-1}$

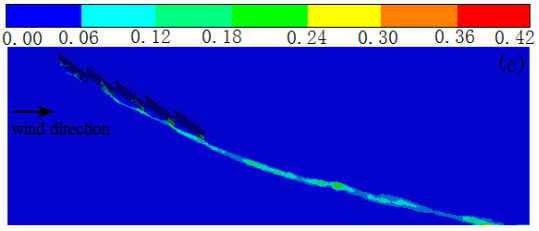

(c) The wind velocity is 12 $m \cdot s^{-1}$

Fig. 9 The eolian contour of the sand Particles to the feather-row engineering when the included angle is 30°

Note: The unit of the scale in the figure is $kg \cdot (m^2 \cdot s)^{-1}$

Because their kinetic energy is low and the bounce distance is short, the wind erosion of the flow to the ground in front of the feather-row engineering is worse. However, the wind erosion to the feather-row wall is weaker and the wind erosion and accumulation areas forming at the tail of the engineering increase. For wind velocities of 10 $m \cdot s^{-1}$ and 12 $m \cdot s^{-1}$, respectively, the kinetic energy of sand particles increases with increasing wind velocity. Furthermore, the bounce distance of sand particles increases accordingly and the wind erosion to the ground in front of the feather-row engineering is lessened, while that toward the feather-row wall increases. Consequently, the wind erosion area forming at the tail of the engineering decreases but the degree increases. Although an increased wind velocity can provide sufficient kinetic energy for the motion of the sand phase in the wind-sand two-phase flow, if wind velocity exceeds 10 $m \cdot s^{-1}$, a small part of sand particles will accumulate at the feather-row and erode the protection area. Therefore, the feather-row transportation engineering will achieve better work efficiency and longer service life under low wind velocity.

3.3 Distribution features of sand particles with different grain diameters

Based on the granular composition and motion features of the wind-drift sand, this study investigated the motion features of the sand particles with maximal saltation in the flow field around the feather-row engineering. The Rosin-Rammler distribution was used to evenly distribute the particle size in a range from 0.1 mm to 0.15 mm. For a wind velocity of 10 $m \cdot s^{-1}$, the motion trail of the sand particles with different particle sizes around the feather-row engineering is shown in Fig. 10.

The motion of sand particles around the feather-row engineering is influenced by both the resistance and transportation force of the engineering. When the included angle between the main shaft of the feather-row engineering and the wind direction is 30°, a small part of the sand particles in front of the feather-row barrier will accumulate at the feather-row engineering. Most sand particles however, will move along the transportation direction at a relatively low bounce height. Most of the sand particles that accumulate at the feather-row engineering have a small particle size. If the included angle between the main shaft of the feather-row engineering and the wind direction is 45°, sand particles with relatively large particle size begin to spill over the feather-row engineering. Some sand particles with small particle sizes spill over the space between adjacent feather-row and move toward the protection area.
The bounce height of the sand particles that move along the transportation direction increases to some extent. For an included angle between the main shaft of the feather-row engineering and the wind direction of 60°, the saltation height of the sand particles motioning in front of the feather-row engineering increases. A large amount of sand particles accumulating at the feather-row engineering or pass the space between adjacent feather-row and move toward the protection area.

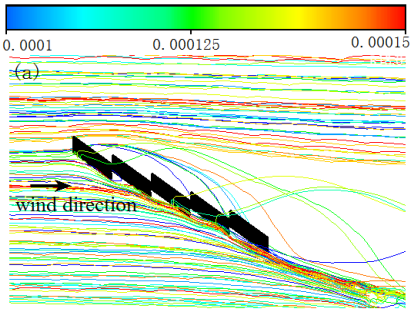

(a) The included angle is 30°

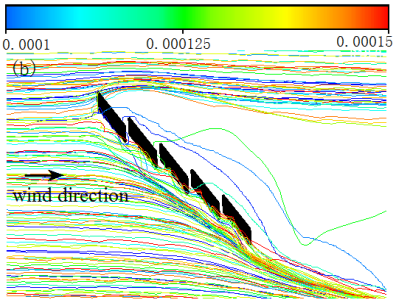

(b) The included angle is 45°

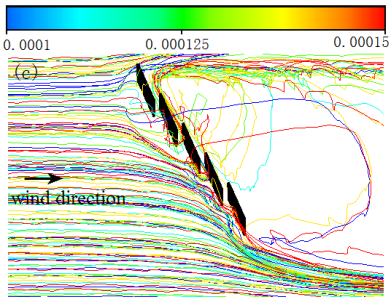

(c) The included angle is 60°

Fig. 10 Motion trail of the sand particles with different sizes passing through the feather-row engineering when the wind velocity is 10 m·s^{-1}

Note: The unit of the scale in the figure is m

At 10 m from the back of the feather-row engineering, a section was chosen with a height of 2 m and an identical width than that of the protection area. The particle size distribution frequency curves of the sand particles passing the section are shown in Fig. 11. When the included angle between the main shaft of the feather-row engineering and the wind velocity is equal, with increasing wind velocity, the particle size distribution frequency curve of the sand particles passing through the protection area is stable. Furthermore, the penetrating frequency of sand particles with different particle sizes tends to be a fixed value. This demonstrates the wind provides kinetic energy for the transportation of the sand particles; however, a higher the wind velocity will decrease the damage to the protection area. When the wind velocity is equal, with increasing included angle between the main shaft of the feather-row engineering and the wind direction, the fluctuations generated by the particle size distribution frequency curve continue to increase and the difference between the frequency extrema passing decreases. This indicates that with the increase of the included angle between the main

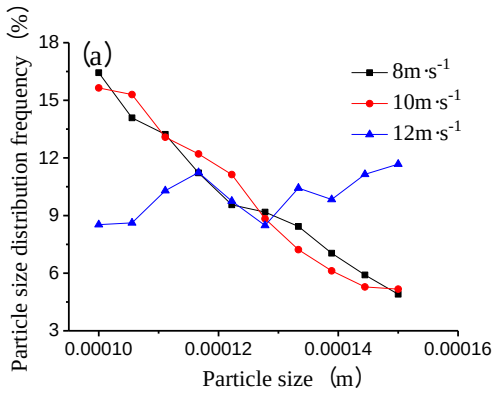

(a) The included angle is 30°

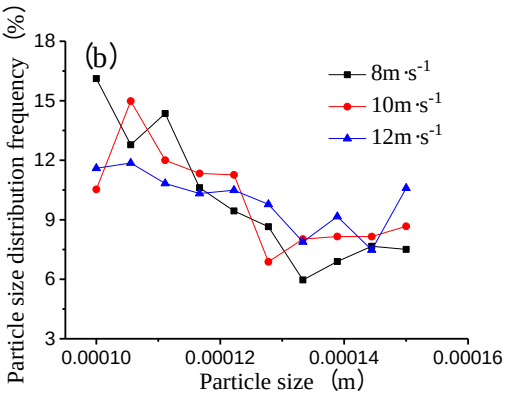

(b) The included angle is 45°

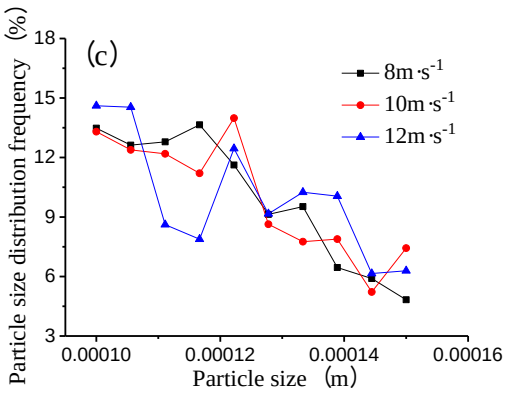

(c) The included angle is 60°

Fig. 11 Distribution frequency curve of sand particles with different particle sizes at the distance of 10m from the back of the feather-row engineering

shaft of the feather-row engineering, the quantity of sand particles spilling over the feather-row engineering continues to increase and the transportation quantity decreases. The smaller the included angle between the main shaft of the feather-row engineering, the less hazardous the wind-sand disasters will be in the protection area.

4. Discussion

According to CFD modeling, the action mechanism of

the feather-row lateral transportation engineering for wind-sand flow differs from that of ordinary sand barriers. As indicated by the obtained simulation results, a transition zone would emerge in front of the feather-row lateral transportation engineering. Its shear velocity would be considerably reduced, causing sand particles in the incoming flow to slow down and deposit. However, with increasing wind velocity, the deposition position of sand particles in front of the feather-row gradually moved backwards. As indicated in Fig. 8, when wind velocity changed from 8 $m \cdot s^{-1}$ to 12 $m \cdot s^{-1}$, sand particles changed from depositing in front of the first feather-row to starting with the first feather-row. The deposition shape of sand particles also thinned and gradually elongated. This suggested that there was a non-deposition length at the head of the feather-row engineering and that its size increased with increasing transportation force of the transportation engineering. Thus, for actual engineering applications, the feather-row engineering should be arranged at the front side of the protection zone, to effectively defend the protection zone and reduce the tail deposition of the engineering.

The formation of wind-sand flow depends on interactions between air and sand, which are two physical media with different densities (Ellis and Sherman 2013). When the wind blows across sandy land, sand particles break away from the land surface due to the wind force. These are then further transported into the air, resulting in the wind erosion of the sandy land and the development of aeolian sand movement. Currently existing numerical models for wind-sand disasters have neglected the formation and migration of aeolian dunes and CFD-based simulations have furthermore ignored the topographic wind fields produced by wind erosion and deposition (Smyth 2016). In fact, this study probes into the transportation engineering of incoming flow blowing across a flat terrain. However, with the deposition of sand in front of the engineering, terrain also changes with the passage of time (Parsons *et al*. 2004). Therefore, the results of this paper apply to terrains without dune coverage on the land surface. Moreover, a transportation engineering is typically combined with sand-retaining and sand-fixing engineerings for sand prevention and control. Thus, future studies should include both the influence of sand-retention and sand-fixing engineerings on the flow field of the transportation engineering. The influence of aeolian sand on the transportation engineering as a result of topographic change should be included as well (Luna *et al.* 2011, Araújo *et al.* 2013) .

During the feather-row engineering design, many factors were found to influence the transportation direction α of the feather-row transportation engineering. These include the angle β between a single feather-row and the prevailing wind direction and the gap a and overlapping length b between adjacent feather-row and the length s1 and width s2 of a single feather-row. Their relationships with the transportation direction α can be written as follows

$$\alpha = \beta - arctan\left(\frac{a + s_2}{s_1 - b}\right) \quad (1)$$

As indicated by Formula (1), given the length s_1 and width s_2 of a single feather-row, to increase the transportation angle and transportation efficiency of the feather-row engineering, it is necessary to adopt a smaller included angle β between a single feather-row and the prevailing wind direction. Furthermore, and larger gap a and overlapping length b between adjacent feather-row in necessary.

5. Conclusions

The research reported here used a 3D numerical simulation to systematically investigate motion features of the wind-sand flow field around the feather-row engineering and sand particles with different particle sizes under different wind velocities. The modelling results are compared to the result obtained by a wind tunnel experiment. The following conclusions can be drawn:

- When the wind-drift sand passes the feather-row engineering and for an included angle between the main shaft of the feather-row lateral transportation engineering and the wind direction of 30°, the achieved transportation effect will be the best. At 45° and 60° included angles, the sand particles moving around the feather-row engineering will decelerate within the deceleration area of the feather-row engineering, move along the transportation direction, and accumulate in the shape of a ridge at the tail of the engineering.
- When the included angle between the main shaft of the feather-row engineering and the wind direction is equal, during the transportation of the wind-drift sand, the wind velocity provides sufficient kinetic energy for the movement of sand particles. With increasing wind velocity, the washout action of the sand particles to the ground and the feather-row engineering intensifies and the transportation quantity and spillover quantity also increase to some extent.
- The resistance and transportation force of the feather-row engineering will change with the change of the included angle between the main shaft of the feather-row engineering and the wind direction. Therefore, when sand particles with different particle sizes move around the feather-row engineering, the particle sizes of the sand particles spilling over the feather-row engineering will increase with increasing included angle between the main shaft of the feather-row engineering and the wind direction. An appropriate included angle between the main shaft of the feather-row engineering and the wind direction can diminish wind-sand disasters in the protection area.

Acknowledgments

This research was supported by the National Natural Sciences Foundation of China (51641808, 51568057, 51268050, 50908152) and the China Postdoctoral Science Foundation (2016M590991). The authors would like to thank the anonymous reviewers and the editor who helped

to improve the quality of this paper.

References

Andrew, F. and Gary, K. (1996), "Toward a model for airflow on the lee side of aeolian dunes", *Sedimentology*, **43**(3), 451-458.

Araújo, A.D., Parteli, E.J.R., Pöschel, T., Andrade, J.S. and Herrmann, H.J. (2013), "Numerical modeling of the wind flow over a transverse dune", *Scientific Reports*, **3**(16), 2858.

Chen, F.Z., Qiang, H.F. and Gao, W.R. (2014), "Simulation of aerolian sand transport with sph-fvm coupled method", *Acta Physica Sinica*, **63**(13), 130202-1556.

Cheng, J.J, Lei, J.Q., Li, S.H.Y. and Wang, H.F. (2016a), "Effect of hanging - type sand fence on characteristics of wind - sand flow fields", *Wind Struct*., **22**(5), 555-571.

Cheng, J.J., Lei, J.Q., Li, S.H.Y. and Wang, F. (2016b), "Disturbance of the inclined inserting - type sand fence to wind - sand flow fields and its sand control characteristics", *J. Aeolian Res*., **21**, 139-150.

Ellis, J.T. and Sherman, D.J. (2013), "Fundamentals of aeolian sediment transport: wind-blown sand", *Treatise on Geomorphology*, 85-108.

Gumaa, Y.T., Haffar, I. and Alafifi, M.A. (1998), "Financial appraisal of date-frond mat fence systems for wind erosion control and sand dune stabilization in the arid region of the united arab emirates", *J. Arid Environ*., **39**(4), 549-557.

Huang, N., Xia, X. and Tong, D. (2013), "Numerical simulation of wind sand movement in straw checkerboard barriers", *Eur. Phys. J. E*., **36** (9), 1-7.

Jackson, D.W.T., Beyers, M., Delgado-Fernandez, I., Baas, A.C. W., Cooper, A.J. and Lynch, K. (2013), "Airflow reversal and alternating corkscrew vortices in foredune wake zones during perpendicular and oblique offshore winds", *Geomorphology*, **187**(5), 86-93.

Kang, L.Q. and Zou, X.Y. (2011), "Vertical distribution of wind–sand interaction forces in aeolian sand transport", *Geomorphology*, **125**(3), 361-373.

Lee, S.J., Park, K.C. and Park, C.W. (2002), "Wind tunnel observations about the shelter effect of porous fences on the sand particle movements", *Atmosph. Environ*., **36**(9), 1453-1463.

Li, B. and Sherman, D.J. (2015), "Aerodynamics and morphodynamics of sand fences: a review", *Aeolian Res*., **17**, 33-48.

Li, S.H.Y. and Lei, J.Q. (2003), "The ecological restoration functions of the straw-checker sand-barriers-A case study along the desert highways in the Gurbantonggut Desert", *Arid Zone Res*., **20**(1), 7-10.

Li, Z., Wang, Y. and Zhang, Y. (2014b), "A numerical study of particle motion and two‐phase interaction in aeolian sand transport using a coupled large eddy simulation – discrete element method", *Sedimentology*, **61**(2), 319-332.

Li, Z.Q., Wang, Y., Zhang, Y. and Wang, L. (2014a), "A random pairing collision model (rpcm) for improving the dem simulation of particle-bed collisions in aeolian sand transport", *Particul. Sci. Technol*., **32**(1), 86-93.

Lima, I.A., Araújo, A.D., Parteli, E.J.R., Andrade, J.S. and Herrmann, H.J. (2017), "Optimal array of sand fences", *Nature - Scientific Reports*, **7**, 45148.

Luna, M.C.M.M., Parteli, E.J.R., Duran, O. and Herrmann, H. J. (2011), "Model for the genesis of coastal dune fields with vegetation", *Geomorphology*, **129**(3-4), 215-224.

Mcclure, S., Kim, J.J., Sang, J.L. and Wei, Z. (2017), "Shelter effects of porous multi-scale fractal fences", *J. Wind Eng. Ind. Aerod*., **163**, 6-14.

Mcewan, I.K., Willetts, B.B. and Rice, M.A. (1992), "The grain/bed collision in sand transport by wind", *Sedimentology*, **39**(6), 971-981.

Murai, H., Alafifi, M.A., Haffar, I. and Yoshizaki, S. (1990), "Use of date-fronds mat fence as a barrier for wind erosion control. 1. effect of barrier density on sand movement stabilization", *Agriculture Ecosyst. Environ*., **32**(3), 273-282.

Parsons, D.R., Wiggs, G.F.S., Walker, I.J., Ferguson, R.I. and Garvey, B.G. (2004), "Numerical modelling of airflow over an idealised transverse dune", *Environ. Model. Softw*., **19**(2), 153-162.

Patankar, N.A. and Joseph, D.D. (2001), "Modeling and numerical simulation of particulate flows by the eulerian–lagrangian approach", *Int. J. Multiphase Flow*, **27**(10), 1659-1684.

Paz, C., Suárez, E., Gil, C. and Concheiro, M. (2015), "Numerical study of the impact of windblown sand particles on a high-speed train", *J. Wind Eng. Ind. Aerod*., **145**(1), 87-93.

Rezaie, S.A. (2009), "Comparison between polylatice polymer and petroleum mulch on seed germination and plant establishment in sand dune fixation", *Iranian J. Range Desert Res*., **16**(134), 124-136.

Rocha, P.A.C., Rocha, H.H.B., Carneiro, F.O.M., Silva, M.E.V. D. and Bueno, A.V. (2014), "K – ω, sst (shear stress transport) turbulence model calibration: a case study on a small scale horizontal axis wind turbine", *Energy*, **65**, 412-418.

Smyth, T.A.G. (2016), "A review of computational fluid dynamics (cfd) airflow modelling over aeolian landforms", *Aeolian Res.*, **22**, 153-164.

Sterk, G., Jacobs, A.F.G. and Van Boxel, J.H. (1998), "The effect of turbulent flow structures on saltation sand transport in the atmospheric boundary layer", *Earth Surf. Proc. Landf.*, **23**(10), 877-887.

Sun, Q.C., Wang, G.Q. and Xu, Y. (2001), "Dem applications to aeolian sediment transport and impact process in saltation", *Particulate Sci. Technol*., **19**(4), 339-353.

Tanière, A., Oesterlé, B. and Monnier, J.C. (1997), "On the behaviour of solid particles in a horizontal boundary layer with turbulence and saltation effects", *Exp. Fluids*, **23**(6), 463-471.

Tian, L., Wu, W., Zhang, D., Lu, R. and Wang, X. (2015), "Characteristics of erosion and deposition of straw checkerboard barriers in alpine sandy land", *Environ. Earth Sci*., 74(1), 573-584.

CC